AMERICAN SOCIETY FOR MICROBIOLOGY | Applied and Environmental Microbiology®

ENVIRONMENTAL MICROBIOLOGY

Differential Phototactic Behavior of Closely Related Cyanobacterial Isolates from Yellowstone Hot Spring Biofilms

Freddy Bunbury,[a] Carlos Rivas,[a] Victoria Calatrava,[a] Amanda N. Shelton,[a] Arthur Grossman,[a] Devaki Bhaya[a]

[a]Carnegie Institution for Science, Department of Plant Biology, Stanford, California, USA

ABSTRACT Phototrophic biofilms in most environments experience major changes in light levels throughout a diel cycle. Phototaxis can be a useful strategy for optimizing light exposure under these conditions, but little is known about its role in cyanobacteria from thermal springs. We examined two closely related *Synechococcus* isolates (*Synechococcus* OS-A dominates at 60 to 65°C and OS-B′ at 50 to 55°C) from outflows of Octopus Spring in Yellowstone National Park. Both isolates exhibited phototaxis and photokinesis in white light, but with differences in speed and motility bias. OS-B′ exhibited phototaxis toward UVA, blue, green, and red wavelengths, while OS-A primarily exhibited phototaxis toward red and green. OS-A also exhibited negative phototaxis under certain conditions. The repertoires of photoreceptors and signal transduction elements in both isolates were quite different from those characterized in other unicellular cyanobacteria. These differences in the photoresponses between OS-A and OS-B′ in conjunction with *in situ* observations indicate that phototactic strategies may be quite versatile and finely tuned to the light and local environment.

IMPORTANCE Optimizing light absorption is of paramount importance to photosynthetic organisms. Some photosynthetic microbes have evolved a sophisticated process called phototaxis to move toward or away from a light source. In many hot springs in Yellowstone National Park, cyanobacteria thrive in thick, laminated biofilms or microbial mats, where small movements can result in large changes in light exposure. We quantified the light-dependent motility behaviors in isolates representing two of the most abundant and closely related cyanobacterial species from these springs. We found that they exhibited unexpected differences in their speed, directionality, and responses to different intensities or qualities of light. An examination of their genomes revealed several variations from well-studied phototaxis-related genes. Studying these recently isolated cyanobacteria reveals that diverse phototactic strategies can exist even among close relatives in the same environment. It also provides insights into the importance of phototaxis for growth and survival in microbial biofilm communities.

KEYWORDS motility, phototaxis, photokinesis, *Synechococcus*, UirS, PixJ, type IV pili, blue light, Octopus Spring, microbial communities, thermophile, cell motility

The laminated microbial mats or biofilms in the outflow channels of hot springs such as Octopus and Mushroom Springs in Yellowstone National Park are ideally suited to examine a dense community of microbes along a stable temperature gradient (1, 2). Between 50 and 70°C, under these mildly alkaline conditions, *Synechococcus* spp. are dominant in the upper few millimeters of the mat (3–7). Light intensity can fluctuate considerably during the day, and it is also rapidly attenuated along with a change in light quality with increasing mat depth due to absorption by pigments such as chlorophylls and bilins (4, 8). The balance of photosynthesis and respiration at different depths sets up gradients of dissolved oxygen and carbon dioxide, which vary over the diel cycle (3, 9–11).

Editor Gladys Alexandre, University of Tennessee at Knoxville

Address correspondence to Devaki Bhaya, dbhaya@carnegiescience.edu.

The authors declare no conflict of interest.

Received 3 February 2022
Accepted 15 March 2022
Published 2 May 2022

Even within the top millimeter of the mat, there is stratification of different *Synechococcus* spp. (or ecotypes) (4, 7, 12), which have different light intensity optima (13). *In situ* measurements of vertical abundance profiles of *Synechococcus* sp. showed that there was a change between day and night, suggesting that this stratification is dynamic, and the rod-shaped *Synechococcus* cells appear to reorient to a vertical position around midday, when light intensities are highest (12). Brock (14) and Carr and Whitton (15) noted that these species were motile, and there is one report from Octopus Spring that measures phototactic gliding motility at the collective level in *Synechococcus* spp. that were named C1 and C9 (16). However, based on 16S rRNA data, these cyanobacteria appear to be most closely related to *Thermosynechococcus elongatus* BP1 (NCBI taxid 197221) and *Gloeomargarita lithophora* (NCBI taxid 1188229), respectively (17), and are relatively rare in these mats (18).

Our knowledge about cyanobacterial phototaxis is mostly derived from the mesophilic, unicellular model organism, *Synechocystis* sp. strain PCC 6803 (referred to here as *Synechocystis*) (19–21). *Synechocystis* requires type IV pili (TFP) for surface-dependent motility (19, 22). It has been demonstrated that light entering a coccoidal *Synechocystis* cell is focused to at least a 4-fold-higher intensity on its opposite side (21), potentially resulting in greater activation of directional photoreceptors. Three photoreceptors, PixJ1 (TaxD1), UirS, and PixD, that influence phototaxis have been characterized in *Synechocystis* (19, 23–25). In *Synechocystis*, motility is also controlled through the cyclic nucleotide second messengers cyclic AMP (cAMP) and c-di-GMP (26–30). Individual *Synechocystis* cells can move over moist surfaces and make phototactic decisions independently, but emergent group behaviors, such as the formation of finger-like projections due to a combination of pilus interactions and the secretion of polymeric substances that facilitate motility, are also observed (31–33). Recent investigations of unicellular cyanobacteria such as *Synechococcus elongatus* PCC 7942 and *Thermosynechococcus vulcanus* suggest that although some components of the phototaxis machinery are similar (e.g., TFP), there may be fine tuning of complex behaviors depending on the environment (34, 35).

Here, we examined two axenic rod-shaped (~3-μm-long, ~1-μm-wide) unicellular cyanobacteria, isolated from Octopus Spring in Yellowstone National Park (6). *Synechococcus* sp. strain JA-3-3Ab (NCBI taxid 321327) (referred to as OS-A here) and *Synechococcus* sp. strain JA-2-3B′a(2-13) (NCBI taxid 321332) (referred to as OS-B′ here) are closely related (96.4% identical 16S rRNA sequences) (36). OS-A predominates at ~60 to 65°C, closer to the spring's source, and has a higher temperature optimum for growth (37), while OS-B′ predominates further downstream at ~50 to 55°C (6, 7) and mostly nearer the surface of the mat (5). Both species absorb light using phycobilisomes composed of phycocyanin and allophycocyanin (36) and exhibit substantial changes in phycobilisome and chlorophyll content under different light conditions (13, 38). We focused on quantifying their motility responses to various wavelengths and intensities of light, at both the single-cell and collective levels, as well as under constant and dynamic light regimens. We found substantial variability within and between the populations in both their photokinetic and phototactic responses. To probe how OS-A and OS-B′ isolates behave in mixed populations, we exposed mixtures to different light regimens, which led to spatial segregation that may reflect their local abundance profiles in the microbial mat. We identified putative homologs of pilus and phototaxis-related genes in the genomes of OS-A and OS-B′. Most of the pilus-related homologs were highly conserved with those in *Synechocystis*, but the photoreceptors were more diverged and also differed between the two isolates. Finally, we attempted to integrate our quantitative characterization of OS-A and OS-B′ light-driven motility with qualitative data from *in situ* studies (7, 16, 39), and discuss the consequences of these differences in the context of the microenvironment that they inhabit.

RESULTS

OS-A and OS-B′ cells move along their long axis and exhibit differences in photokinesis and phototaxis. To measure the phototactic responses of OS-A and OS-B′, cells from actively growing liquid cultures were spotted on low-concentration (0.4%)-agarose plates and incubated at 50°C under constant directional white light of

60 μmol·m^{-2}·s^{-1} (see Fig. S1 for the spectrum). We observed that OS-A and OS-B′ cells exhibited little to no motility over the first few hours after plating but started to move and form projections extending toward the light within 1 to 3 days. We observed that these finger-like projections, indicative of population-level positive phototaxis, frequently had a sinuous appearance at the leading edge or merged to form a continuous front (Fig. 1A). In some cases, described below (see Fig. 3 and 4), we observed transient negative phototaxis. To quantify the short-term behavior of single cells, we tracked individual cells within these projections using time-lapse video microscopy (TLVM) over periods of 4 to 10 min. Example videos can be found at https://www.youtube.com/channel/UCX0gm-79tZplREzHteapEWA. Figure 1B illustrates a typical example where we tracked the phototactic movement of OS-A and OS-B′ cells toward 70 μmol·m^{-2}·s^{-1} white light coming from the right side of the image, with colored tracks indicating their path over the previous 2 min. These tracks and the cell outlines allowed us to quantify how they moved relative to their cell axis as well as their phototactic (directional) and photokinetic (speed) responses to light.

First, we determined that both OS-A and OS-B′ isolates moved predominantly parallel to their long axis, with OS-A, in particular, rarely deviating from this type of movement, by measuring the average angle between their long axis and the direction in which they moved (Fig. S2). Second, we quantified the average speed of OS-A and OS-B′ cells in darkness over the entire period in which they were tracked (Fig. 1C). Most OS-A cells exhibited little motility in the dark (mean speed of 0.07 μm·s^{-1}), although the speed distribution appeared bimodal, with peaks representing motile (right peak) and essentially immotile (left peak) cells. OS-B′ cells moved more than three times faster (mean speed of 0.25 μm·s^{-1}). After directional illumination (measured between 60 and 120 s after illumination) with white light at 70 μmol·m^{-2}·s^{-1}, OS-A cells significantly increased their speed to 0.12 μm·s^{-1} (Kolmogorov-Smirnov $P < 0.001$), while OS-B′ cells did not (0.26 μm·s^{-1}, $P = 0.06$). Third, to quantify the direction of their movement, we selected cells that showed obvious motility (>0.05 μm·s^{-1}) and plotted their directions on a rose plot (Fig. 1D). In the dark, neither OS-A nor OS-B′ showed any directional bias (Rayleigh test $P > 0.05$). Under directional illumination, OS-A cell motility was substantially biased toward the light source ($b = 0.34$, $P < 0.001$), and to a lesser extent, so was OS-B′ ($b = 0.19$, $P < 0.001$). Decreasing illumination from 70 to 4 μmol·m^{-2}·s^{-1} reduced the mean speed of OS-A cells from 0.15 to 0.09 μm·s^{-1} (Fig. S3) but had no significant effect on OS-B′. Motility bias decreased from 0.29 to 0.07 in OS-A and decreased from 0.17 to 0.03 in OS-B′ when illumination was decreased from 70 to 4 μmol·m^{-2}·s^{-1} (Fig. S4). In summary, both OS-A and OS-B′ mainly moved parallel to their long axis, but OS-A cells were less motile in the dark and more responsive to light than OS-B′, showing greater photokinetic (increase in speed) and phototactic (positive directional bias) responses upon illumination.

OS-A and OS-B′ exhibit different motility dynamics in response to changing light conditions. Next, we asked if OS-A and OS-B′ showed similar responses to sudden changes in light levels (such as those experienced on a cloudy day in their natural environment). We tracked cell motility during transitions from dark to light and back to dark conditions (each period lasting 2 min). OS-A cells increased their speed (photokinesis) by approximately 2.5-fold within 10 to 20 s after transitioning to the light. This peak speed appeared to be transient and dropped after about 30 s to an intermediate level (2-fold higher than the initial speed) that was maintained throughout the light period (Fig. 2A). Transitioning to the dark caused a decrease in speed within 20 s to a level even lower than at the start, followed by a gradual recovery that was still not complete after the 2-min dark period. For OS-B′, there was no significant change in speed upon illumination, but a transition to the dark caused a substantial drop to 50% of the original speed, which then mostly recovered to the starting speed within the 2-min dark period.

OS-A exhibited no motility bias in the dark but showed a rapid increase in bias toward the light within 30 s of illumination and then a more gradual increase to a maximum motility bias of 0.4, after 2 min (Fig. 2B). Within 60 s after transitioning to

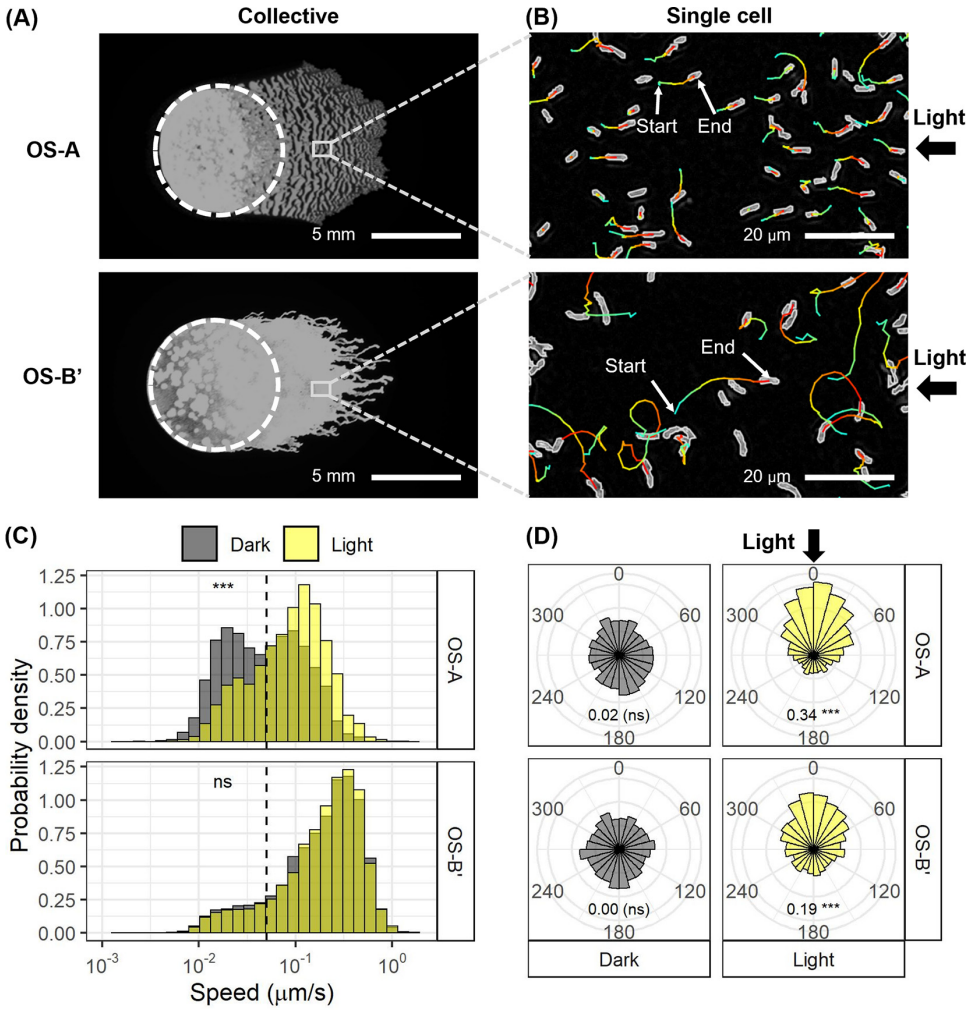

FIG 1 OS-A and OS-B′ cells exhibit differences in photokinesis and phototaxis. (A) Chlorophyll fluorescence scan of droplets of *Synechococcus* cells plated on DH10 medium with 0.4% agarose and incubated for 4 days at 50°C under directional (right of image) 60-μmol·m^{-2}·s^{-1} white light. White dashed circles indicate the original position of the droplet after plating. Gray boxes show areas magnified in panel B (indicated by the dashed lines) and are the approximate areas in which single-cell motility measurements were made (not to scale). (B) Single cells were tracked by time-lapse video microscopy (TLVM) recorded for 2 min at ×200 magnification and 10 frames per min under directional (right of image) 70-μmol·m^{-2}·s^{-1} white light. Cells (outlined in gray) and cell trajectories that were successfully tracked from start (blue) to end (red) of the 2-min period are shown. One cell track for each isolate is annotated with "start" and "end" arrows. Note the considerable variability in the track length and trajectory. If cell trajectories could not be successfully tracked for the full 2 min, their tracks were eliminated from the image. Full-length tracks were used to calculate speed and direction of the cells in panels C and D, respectively, with recording at 50°C for 1 min in the dark and light (from minute 1 to 2 after transition to light) at 10 frames per min. (C) Density plots showing the proportion of cells moving at different speeds in the dark (1.5 μmol·m^{-2}·s^{-1} from the microscope light) (gray distributions) and 70 μmol·m^{-2}·s^{-1} white light (yellow distributions). Black dashed lines indicate 0.05 μm·s^{-1} (the speed above which cells were selected for analysis of motility bias in panel D). Kolmogorov-Smirnov test performed on the difference in speed distributions in the dark and light indicates a significant difference in OS-A (***) but not OS-B′ (ns). n = 3,100 to 4,200 cells per distribution. (D) Rose plots indicating the proportion of cells moving at >0.05 μm·s^{-1} on average in each direction, split into 15°-wide segments. Direction of cell movement is shown for OS-A and OS-B′ in the dark (gray plots [left]) and under white light (70 μmol·m^{-2}·s^{-1}) (yellow plots [right]). The illumination is from the top (0°). Values at the bottom of each rose plot indicate motility bias (net proportion of movement in the direction of the light source), with asterisks indicating statistical significance according to a Rayleigh test (***, $P < 0.001$; ns, not significant, i.e., $P > 0.05$). n = 1,500 to 3,700 cells per distribution.

darkness, the motility bias decreased to 0. Motility bias in OS-B′ responded similarly: it started at 0 in the dark, rose rapidly at first, plateaued at 0.2 on illumination, and then declined to 0 within 40 s after the light was turned off. OS-A had a sharper rise and greater maximum motility bias than OS-B′, which appeared to still be increasing at the end of the 2-min light period. Short time periods were chosen to allow multiple

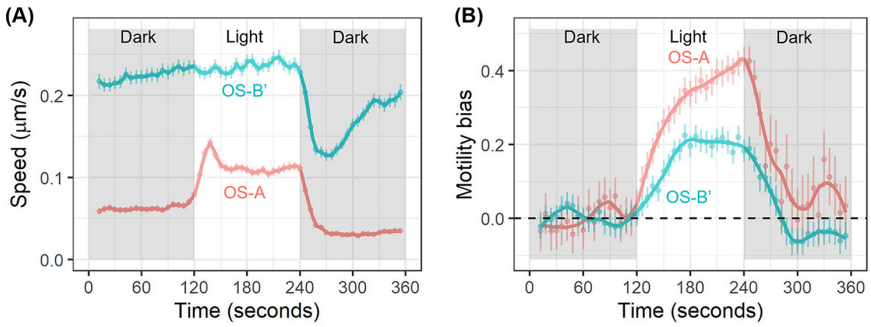

FIG 2 OS-A and OS-B′ exhibit different motility dynamics under changing light conditions. Individual cells within finger-like phototactic projections (formed on motility plates) were captured by TLVM at 10 frames per min at 50°C, over a 6-min period with 2 min each of darkness, white light (70 μmol·m^{-2}·s^{-1}), and darkness again, and their velocities (speed and direction) were calculated. Points represent mean values of cells from 16 biological replicates (average of 2,700 cells per time point for panel A and 1,350 cells per point for panel B). Error bars represent the 95% confidence intervals of the means, and lines are a local regression smoothing over the points. Red, OS-A; blue, OS-B′. (A) Mean speed of cells, in μm·s^{-1}. (B) Mean motility bias (net proportion of velocity directed toward the light) of cells with a speed of >0.05 μm·s^{-1}.

replicates to be tested so that results would be broadly representative of OS-A and OS-B′ phototactic behavior. Further experiments would be necessary to determine the longer-term dynamics and acclimation to changing light conditions.

Population-level phototaxis of OS-A and OS-B′ is controlled by both light intensity and quality. The behavior of cell populations cannot be predicted or extrapolated from single-cell motility measurements. So, to quantify population-level phototaxis, we measured the maximum length of phototactic projections each day over a 10-day period during incubation under directional light (an example is shown in Fig. 1A). To choose experimental conditions that would be optimal for testing the effect of light over several days, we checked the effect of surface stiffness and moisture (agarose concentration) and cell density. Increasing agarose percentage reduced motility of both strains, while increasing cell density had a positive effect (Fig. S5). Using these data, we decided to perform experiments with *Synechococcus* cells at an adjusted optical density at 730 nm (OD_{730}) of 8 plated on DH10 medium solidified with 0.4% agarose.

We measured the effect of light intensity on collective phototaxis at 2-fold-increasing intensities from 2.5 μmol·m^{-2}·s^{-1} up to 640 μmol·m^{-2}·s^{-1} over a 10-day period. Figure 3A indicates the daily displacement of the most positively phototactic and negatively phototactic (if any) projections, and Fig. 3B illustrates a representative example of these projections on day 2. At the midpoint of the measurements (day 5), OS-A phototactic projections had moved furthest (6 mm) at 40 to 80 μmol·m^{-2}·s^{-1}, while OS-B′ phototactic projections had moved furthest (13 mm) at 10 μmol·m^{-2}·s^{-1}. At 80 to 160 μmol·m^{-2}·s^{-1}, OS-A had moved further than OS-B′, but at the lower intensities of 2.5 to 40 μmol·m^{-2}·s^{-1}, OS-B′ had moved further. Between 80 and 320 μmol·m^{-2}·s^{-1}, a small portion of the OS-A cells exhibited transient negative phototaxis. These negatively phototactic projections were thinner, appeared earlier than positive phototactic projections, and often either stopped or reversed direction within a few days (a similar result was reported for other *Synechococcus* species from Octopus Spring by Ramsing et al. [16]). Above 80 μmol·m^{-2}·s^{-1} for OS-B′ and above 320 μmol·m^{-2}·s^{-1} for OS-A, no finger-like projections were observed, and toward the end of the growth period, we observed that both isolates had bleached above 160 μmol·m^{-2}·s^{-1}.

Next, we quantified the phototactic responses of OS-A and OS-B′ under specific wavelengths of light (red [630 nm], green [520 nm], blue [450 nm], and UVA [360 nm]) at intensities varying between 5 and 320 μmol·m^{-2}·s^{-1}. As with the white-light experiments, we illustrate the daily displacement of the phototactic projections (Fig. 4A) and present a representative example of these on day 2 (Fig. 4B). OS-A exhibited phototaxis in green light (maximal at 80 μmol·m^{-2}·s^{-1}) and red light (maximal at 10 μmol·m^{-2}·s^{-1}), but no phototactic projections were observed under blue or UVA radiation (OS-A cells showed

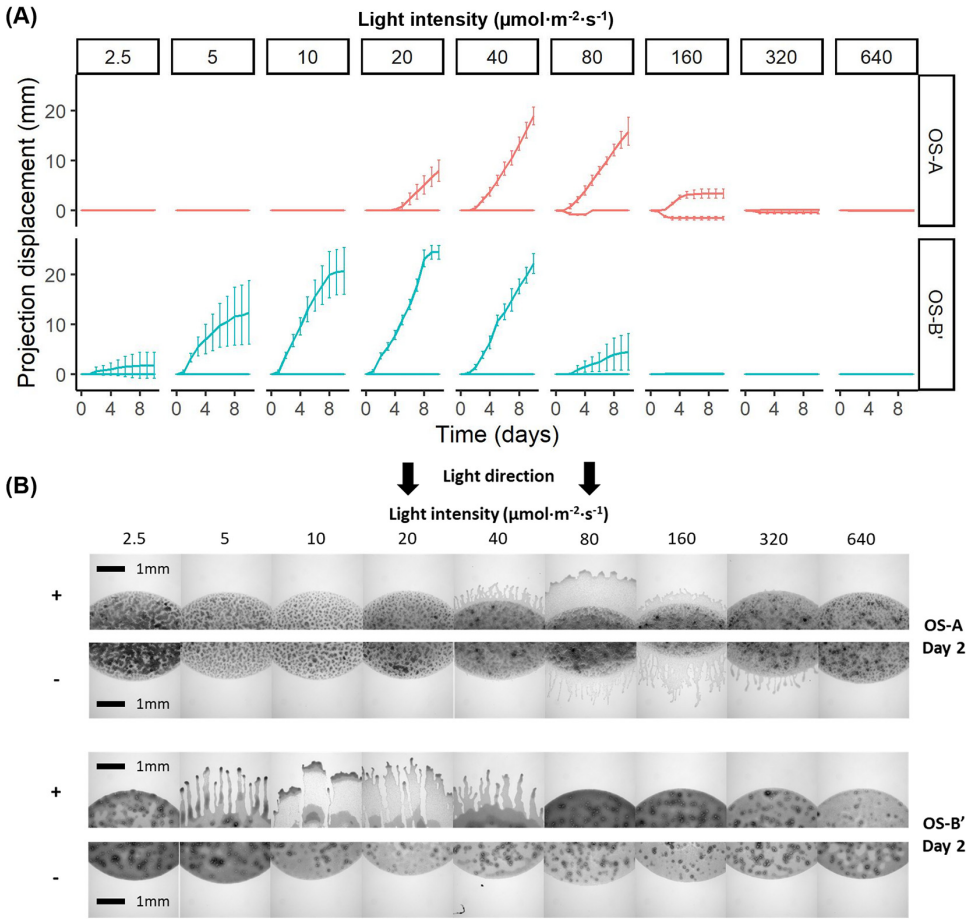

FIG 3 Light intensity affects the collective phototaxis of OS-A and OS-B′. Motility assays were performed as described in Materials and Methods with exposure to unidirectional white light (composed of red, green, and blue peaks) (Fig. S1B) at 2.5, 5, 10, 20, 40, 80, 160, 320, and 640 μmol·m^{-2}·s^{-1} for 10 days. (A) The distance from the initial proximal or distal edge of the drop to the longest finger-like projection extending toward (upper line) or away from (lower line) the light, respectively, was measured daily (note that under many conditions, one or both lines are horizontal, indicating that no phototaxis occurred). Red, OS-A; blue, OS-B′. Error bars represent the 95% confidence intervals of the means from 8 biological replicates. The edge of the plate is 25 to 30 mm from the initial edge of the droplet; hence, there is an apparent slowing down by day 8 to 10 of the most phototactic projections. (B) Bright-field images were acquired for a representative OS-A replicate (top) and OS-B′ replicate (bottom) after 2 days of incubation at ×50 magnification of the edge of the droplet/phototactic projections closest to (top [+]) and furthest from (bottom [−]) the light source.

pronounced flocculation in blue light, but we did not explore this phenomenon further). OS-A cells also exhibited transient negative phototaxis under red light (10 to 20 μmol·m^{-2}·s^{-1}) and green light (40 to 160 μmol·m^{-2}·s^{-1}). In OS-B′, maximal positive phototaxis occurred in green and red light (as for OS-A) but at lower intensities: 20 μmol·m^{-2}·s^{-1} and 5 μmol·m^{-2}·s^{-1} for green and red, respectively. However, unlike OS-A, negative phototaxis was not observed. Another striking difference was that unlike OS-A, OS-B′ showed phototaxis in both blue and UV-A light, although the phototactic projections slowed or halted more quickly than under red or green light. In summary, only OS-A exhibited negative phototaxis, while OS-B′ was more positively phototactic and over a wider range of wavelengths and intensities, and both species moved further under green and red light than blue or UVA radiation.

These long-term motility experiments indicated that there are several differences in the responses of OS-A and OS-B′ cells to both wavelength and light intensity that were observed over a time course of several days. To test whether OS-A and OS-B′ cells have an initial response to different wavelengths of light, we used the single-cell motility assay described above. Surprisingly, while no collective phototaxis was observed for

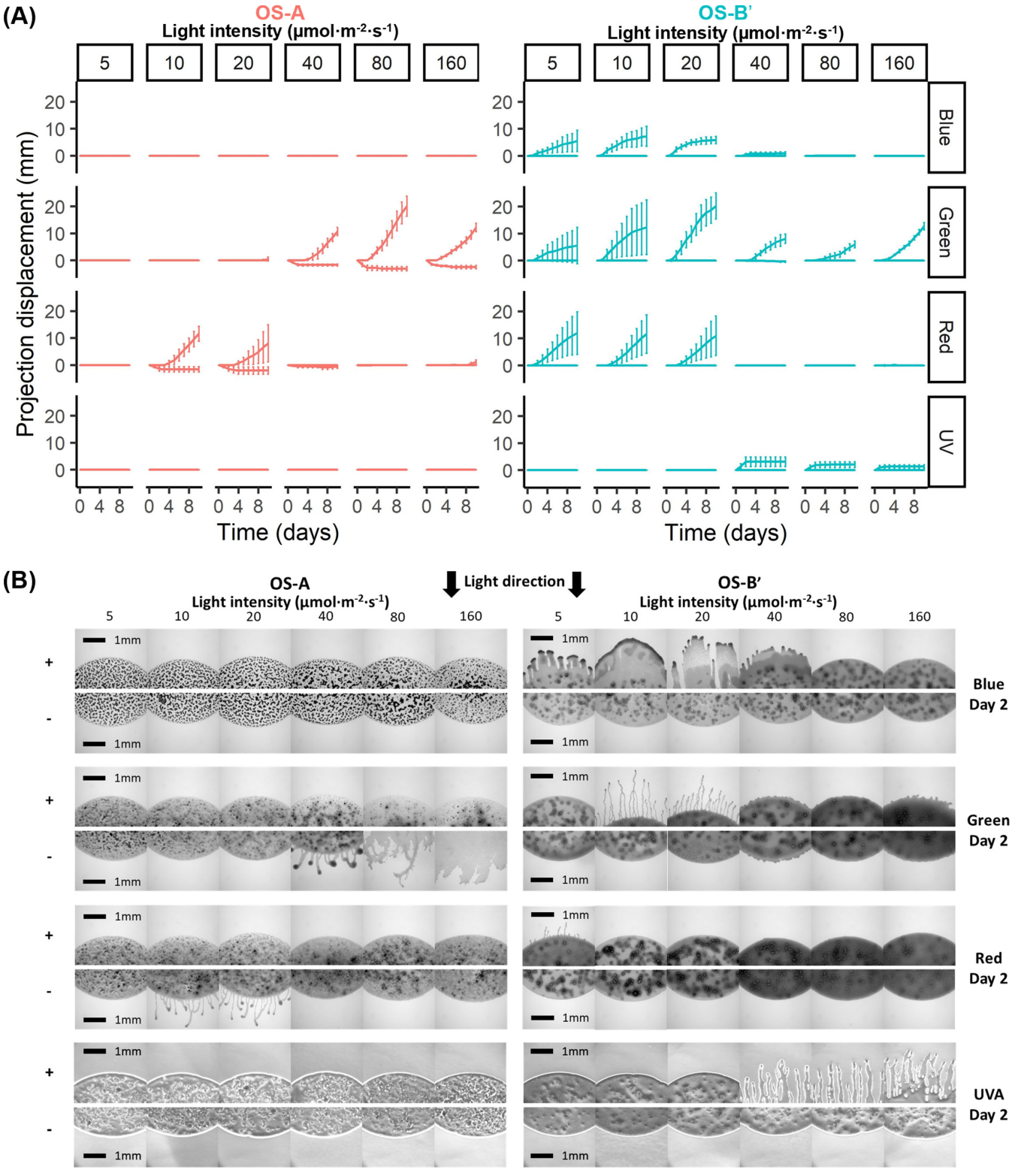

FIG 4 Light intensity and wavelength affect the collective phototaxis of OS-A and OS-B′. Motility assays were performed as described in Materials and Methods with exposure to blue (450 nm), green (520 nm), red (630 nm), or UV (370 nm) light at 5, 10, 20, 40, 80, or 160 μmol·m^{-2}·s^{-1} for 10 days. (A) The distance from the initial proximal or distal edge of the drop to the longest finger-like projection extending toward (upper line) or away from (lower line) the light, respectively, was measured daily (note that under many conditions, one or both lines are horizontal, indicating that no phototaxis occurred). The light colors are listed on the right. Error bars represent the 95% confidence intervals of the means from 8 biological replicates. (B) Representative OS-A droplet (left) and OS-B′ droplet (right) after 2 days of incubation showing the edge of the droplet/phototactic projections closest to (top [+]) and furthest from (bottom [−]) the light source.

OS-A in blue light, there was a substantial transient increase in speed (4-fold) and motility bias (to 0.2) at the single-cell level (Fig. S6). Moreover, while OS-B′ collectively moved toward blue light (Fig. 4), single-cell speed decreased transiently upon illumination (although it remained higher than that in OS-A, which decreased consistently under increasing intensities of blue light) and motility bias was lower than in OS-A (Fig. S6). Both OS-A and OS-B′ showed positive phototaxis at low intensities and negative phototaxis at high intensities of blue light, with the switch occurring at 35 μmol·m^{-2}·s^{-1} for OS-B′ and 65 μmol·m^{-2}·s^{-1} for OS-A (Fig. S6). Under green and red light, the change in speed was less marked, although it appeared to increase with intensity, and no substantial effect on motility bias was observed for either isolate even though under these conditions at the collective level, both isolates formed long positive phototactic projections (Fig. 4A).

Mixed populations of OS-A and OS-B′ segregate under different light regimens. *In situ* studies in Octopus Spring microbial mats showed that OS-A and OS-B′ have differential abundances along the depth profile, with OS-B′ being most abundant from 0 to 500 μm, while OS-A abundance peaked at approximately 600 μm below the surface (16). To test whether these different depth profiles might in part be driven by phototaxis, we incubated OS-A and OS-B′ separately as well as in a 1:1 mixture (each isolate at half the density) under directional white light at either 5 or 80 μmol·m^{-2}·s^{-1}. Our results (Fig. 3 and 4) suggested that these conditions would favor the motility of OS-B′ and OS-A, respectively. As expected, after 5 days in directional light, we found that under 5 μmol·m^{-2}·s^{-1}, OS-B′ moved considerably further than OS-A (Fig. 5A). Under 80 μmol·m^{-2}·s^{-1}, OS-A moved slightly further than OS-B′. Under the higher light intensity, both isolates visibly appeared to reach a greater density and extend toward the light in a more continuous front rather than finger-like projections under the lower intensity (Fig. 5A). To establish whether there was differential motility between isolates in the mixed samples, we needed to distinguish between the morphologically similar OS-A and OS-B′ cells. To do so, we performed qPCR using primers specific for OS-A or OS-B′ (Table 1) on DNA extracted from the cells sampled from five regions along the phototaxis projection, as shown by white rectangles in Fig. 5A.

Under 5 μmol·m^{-2}·s^{-1}, the OS-A/OS-B′ ratio did not vary considerably from the far side of the droplet to the midpoint of the finger-like projections (positions 1 to 4). However, at the tips of the projections (position 5), there was significant enrichment of OS-B′ (Fig. 5B). Conversely, at 80 μmol·m^{-2}·s^{-1}, OS-A was enriched at the tips. Throughout most of the sampling region under 80 μmol·m^{-2}·s^{-1}, however, OS-B′ was more abundant than OS-A, particularly at the midpoint of the finger-like projections. We attribute this to a combination of higher growth rate of OS-B′ at 50°C than OS-A (37) and the fact that a larger proportion of population appeared phototactic than in OS-A (Fig. 3 and 5). Both isolates were present at all sampling points despite particularly substantial differences in phototaxis at the lower (5μmol·m^{-2}·s^{-1}) light intensity. This suggests that certain strains could move through mixed communities without necessarily contributing to the pool of motility-promoting substances (or "slime") (33, 40) as long as they exhibit a motility bias.

OS-A and OS-B′ have homologs of only a subset of the phototaxis-related genes characterized in *Synechocystis*. Several photoreceptors and members of the signal transduction network required for phototaxis were initially identified and characterized in the model cyanobacterium *Synechocystis* (19, 24, 41). The amino acid sequences of these proteins were used to identify homologs in OS-A and OS-B′. The *Synechocystis* genome contains three chemotaxis-like operons (*Tax1* to *-3*), of which *Tax1* is involved in positive phototaxis and *Tax3* in pilus biogenesis (42). We identified putative homologs via reciprocal protein best BLAST hits to the genes in the *Tax1* and *Tax3* loci but not the *Tax2* locus (Table S2). There are three cyanobacterial photoreceptors known to play a role in phototaxis: PixJ (also known as TaxD1), UirS, and PixD (19, 24, 25). PixJ and UirS have homologs in OS-A (CYA_2156-9 and CYA_2553) and OS-B′ (CYB_2751 and CYB_1773), but none were found for PixD or its response regulator PixE. In *Synechocystis*, motility is modulated by the concentration of the cyclic nucleotide

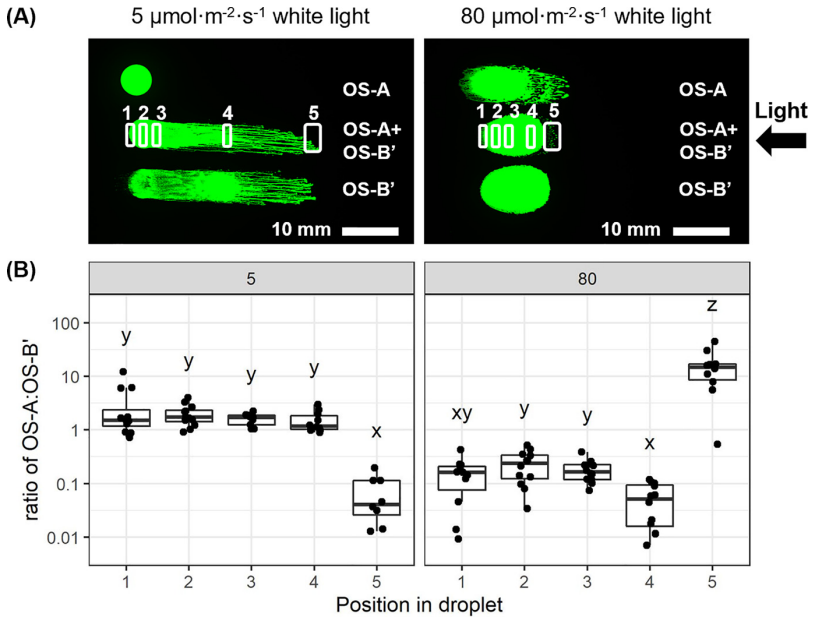

FIG 5 Mixed populations of OS-A and OS-B′ segregate under different light regimens. Motility assays were performed as described in Materials and Methods with exposure to white light at 5 or 80 μmol·m^{-2}·s^{-1} for 5 days. OS-A and OS-B′ were spotted axenically and in a 1:1 mixture. (A) Scans of the phototactic cells were made after 5 days, and samples were collected from the five regions indicated by the white rectangles, which correspond to negative phototactic fingers, if any, or otherwise the distal end of the droplet (box 1), the center of the droplet (box 2), the proximal edge of droplet (box 3), the midpoint of positive phototactic projections (box 4), and the tip of positive phototactic projections (box 5). (B) Genomic DNA was extracted and qPCR performed using primers specific to regions in the *psaA* gene unique to either OS-A and OS-B′ (Table 1). The ratio of OS-A to OS-B′ in each sample was calculated from qPCR threshold cycle values and is presented on a log scale (*y* axis), with the left and right plots representing samples incubated under 5 and 80 μmol·m^{-2}·s^{-1}, respectively. Letters indicate statistical differences at a *P* value of <0.05 in group medians (box plots in the same panel that share one or more letters are not significantly different, and those that do not share a letter[s] are significantly different). Pairwise *P* values were calculated by Kruskal-Wallis and *post hoc* Dunn tests with Benjamini-Hochberg false discovery rate correction. $n = 9$ to 12 biological replicates.

second messengers cAMP and c-di-GMP, which are produced by Cya1 and Cph2 (among others), respectively (27, 29). Homologs of Cya1 and the cAMP-binding transcriptional activator Sycrp1 were both found in OS-A (CYA_2405 and CYA_1331) and OS-B′ (CYB_2200 and CYB_2652). No homolog of Cph2 was found in either OS-A or OS-B′. Nonetheless, we did find some genes with predicted diguanylate cyclase (GGDEF) and phosphodiesterase (EAL) domains, which may alter c-di-GMP levels. OS-A encoded one protein with a single EAL domain (CYA_1130), which showed similarity to stand-alone bacterial EAL domain proteins involved in cell motility and biofilm formation (43), while the OS-B′ genome lacked any predicted EAL domains. In contrast,

TABLE 1 Primers used in this study[a]

Primer name	Purpose	Sequence
76_OSB_psaA_F	OS-B′ quantification	GTTGATCCCGGACAAAGGCAAATT
77_OSA_psaA_F	OS-A quantification	CTGATCCCCGATAAGGCCAAG
78_OSB_psaA_R	OS-B′ quantification	GTGGAAGATCACGATGGAGATGCA
79_OSA_psaA_R	OS-A quantification	GGAAGATCACAATCGAGATGGCG
101_Syn_PsaA_2F	OS-A vs. OS-B′ identification	TCATGGCGTACATGTGCTGC
102_Syn_PsaA_2R	OS-A vs. OS-B′ identification	CAAGTGGTCTGGCCCATCTT
155_Syn_16S_F	OS-A vs. OS-B′ identification	GATGAGCCTGCGTCGGATTA
158_Syn_16S_R	OS-A vs. OS-B′ identification	CTTTGTCCGCGCCATTGTAG

[a]Primers were used for quantification of OS-A and OS-B′ from mixed phototactic projections using qPCR and for amplification of the 16S and PsaA regions for Sanger sequencing to confirm the identity of the strains as OS-A and OS-B′.

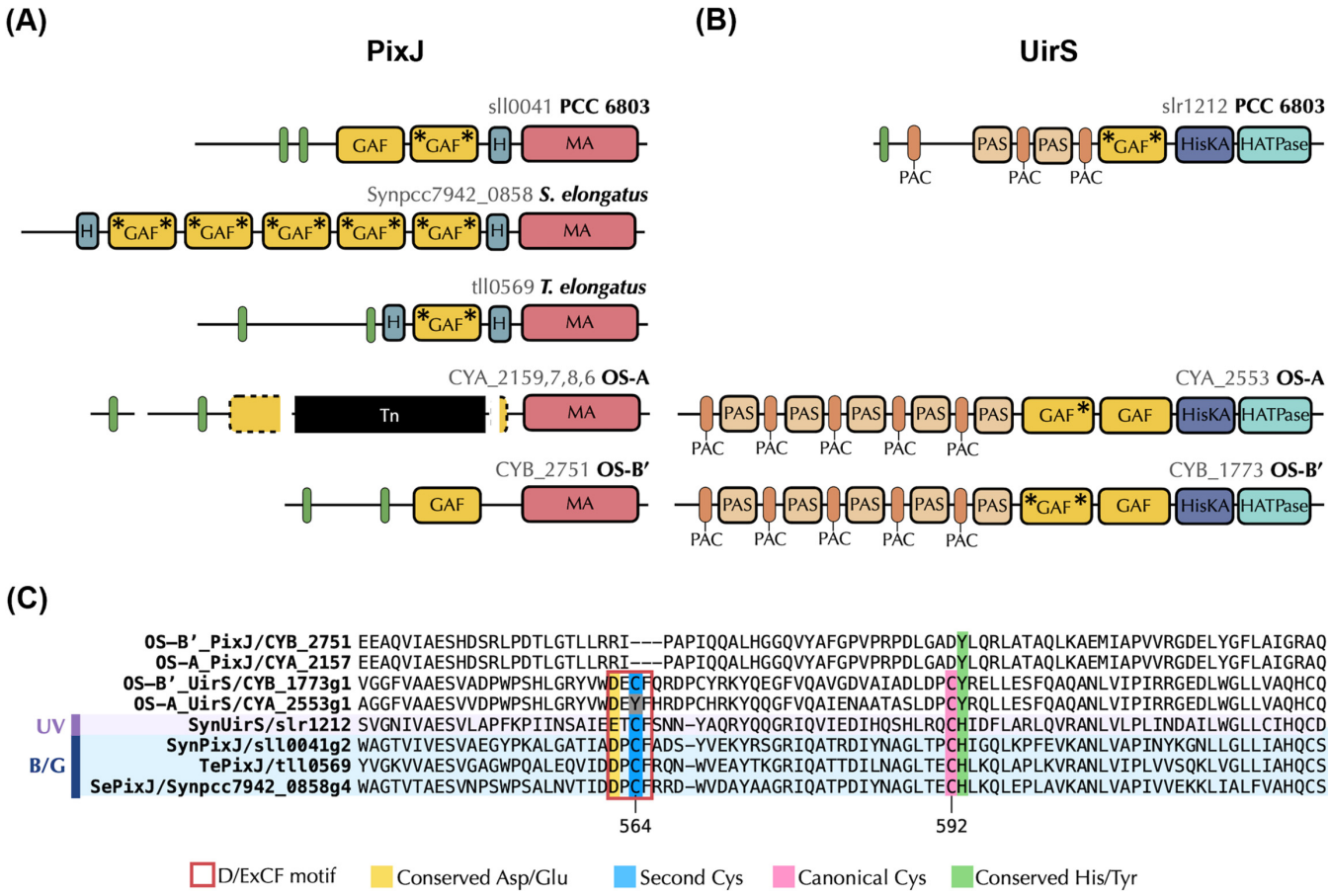

FIG 6 OS-A and OS-B′ encode possible homologs of the *Synechocystis* phototaxis photoreceptors, PixJ and UirS. (A) Conserved domains within PixJ homologs in *Synechocystis* sp. strain PCC 6803, *Synechococcus elongatus* PCC 7942, *Thermosynechococcus elongatus* BP-1, and OS-A (split into 4 open reading frames) and OS-B′: transmembrane domain (green bars), HAMP domain (blue bars labeled "H"); cGMP phosphodiesterase/adenylate cyclase/FhlA domain for photoreception (yellow boxes labeled "GAF"), methyl-accepting chemotaxis-like domain (red boxes labeled "MA"), conserved bilin-binding Cys residues (asterisks), and ISSoc1 transposase (black box labeled "Tn"). (B) Conserved domains within UirS homologs in *Synechocystis*, OS-A, and OS-B′ (not found in *S. elongatus* or *T. elongatus*). Beige box labeled "PAS," period circadian, Ah receptor nuclear translocator, single-minded domain; orange box labeled "PAC," PAS C-terminal domain; dark blue box labeled "HisKA," dimerization and phosphoacceptor domain of histidine kinase; light blue box labeled "HATPase," histidine kinase-, DNA gyrase B-, and phytochrome-like ATPases. (C) Alignment of conserved bilin-binding region within the GAF domains of the homologs illustrated in panels A and B. For proteins with multiple GAF domains, we selected the GAF domain shown to be involved in bilin binding or directional photoperception or to have the conserved cysteines. Species, gene name, and the relative GAF domain position (1 to 5) are indicated to the left of each sequence. GAF domains with characterized responses to blue/green and UV light are highlighted in blue and purple, respectively. Relevant conserved residues are colored or boxed according to the key below the protein alignments. Numbers indicate amino acid residue positions in *Synechocystis* PixJ.

GGDEF domains were found in both isolates: in three OS-B′ proteins (CYB_0347, CYB_2277, and CYB_2163) and two orthologous OS-A proteins (CYA_0483 and CYA_2618). The third (nonorthologous) member in OS-B′ contains a PAS and a GAF domain at the N terminus (CYB_2163), although this domain does not have the conserved bilin-binding Cys residues.

The putative homolog of the blue/green photoreceptor PixJ in OS-A and OS-B′ showed low sequence similarity (<50% coverage and amino acid identity) to *Synechocystis* PixJ and, importantly, lacked the two conserved cysteine residues within the GAF domain that are essential for covalently binding the chromophore (Fig. 6A; Table S2) (44, 45). In addition, in OS-A, this gene is disrupted by insertion of an ISSoc1 transposase. By comparison, the GAF domains in the PixJ homologs in *S. elongatus* and *T. elongatus* contain amino acid sequences flanking these bilin binding cysteines that are highly conserved with *Synechocystis* (Fig. 6C). This suggests that neither OS-A nor OS-B′ encodes a functional PixJ homolog, although this has yet to be demonstrated experimentally. The UV-A/green-light receptor UirS in *Synechocystis* contains one GAF domain with two conserved cysteine residues (46). Both OS-A and OS-B′ appear to

contain a UirS homolog (31% amino acid identity, 52% coverage), but unlike UirS in *Synechocystis*, they contain two GAF domains. Of these, the first GAF domain contains one cysteine in OS-A and both cysteines in OS-B′, while the second GAF domain in both OS-A and OS-B′ lacks both bilin-binding cysteines (Fig. 6B and C). Furthermore, the UirS homolog in both OS-A and OS-B′ has additional putative sensing elements (five PAC-PAS domains, which can also potentially interact with a chromophore) at its N terminus. Homologs for the downstream molecular elements involved in signal transduction through UirR and LsiR in *Synechocystis* were not found in OS-A nor OS-B′. Further experiments will be required to identify the signal transduction network in OS-A and OS-B′, but there are several differences in the networks of these closely related organisms that may reflect their microenvironment.

DISCUSSION

The motivation for this study was to examine the light-dependent motility responses in related and coexisting thermophilic cyanobacteria and to correlate these responses with their physical environment and the signal transduction network controlling phototaxis. Surprisingly, the two dominant *Synechococcus* isolates (OS-A and OS-B′) in these mats exhibited distinct responses to various light intensities and wavelengths and differences in their short-term responses to changing light conditions as well as their long-term collective behaviors (7). We compared their gene repertoire to genes known to control phototaxis in *Synechocystis* (19, 24, 25) and found that PixJ is unlikely to be active and PixD is absent, suggesting that the putative homolog of UirS may function as a photoreceptor. Finally, we attempted to correlate these photoresponses with previous results from *in situ* studies (12). There have been only a few studies of phototaxis in recently isolated environmental strains. These include *Thermosynechococcus elongatus*, *Thermosynechococcus vulcanus*, *Synechococcus elongatus* (UTEX 3055), and *Synechococcus* isolates C1 and C9 from Yellowstone hot springs (16, 34, 35, 47). Our results complement these studies (selected results are summarized in Table 2) and suggest that phototactic responses have evolved in the context of the local physical environment. The repertoire of photoreceptors and signaling components appear to show evolutionary plasticity and to have evolved to tune light-dependent motility responses.

Comparison of phototactic and photokinetic responses in thermophilic *Synechococcus* spp. and other cyanobacteria. Tracking the movement of individual OS-A and OS-B′ cells in the dark or light revealed that they had a broad distribution of cell speeds, with many cells remaining immotile (Fig. 1C). This is similar to behavior observed in *Synechocystis* (48). On transition from darkness to 70 μmol·m^{-2}·s^{-1} light, OS-A showed a 2-fold increase in speed (Fig. 2A), which is similar to that observed in *Synechococcus* C1 and C9 and *Synechocystis* (16, 49). However, OS-B′ did not exhibit a significant difference in photokinesis upon illumination, similar to that reported in *T. elongatus*, *S. elongatus* (UTEX 3055), and *Synechocystis* ATCC 27184 isolates (34, 47, 49). Speed in both OS-A and OS-B′ cells declined to a minimum at around 40 to 60 s after the transition from light to darkness. In contrast, the speed of *Synechocystis* cells did not appear to decrease upon transfer to darkness (49, 50). Reports of the dynamic responses of *Synechocystis* to illumination generally agree that phototactic orientation toward the light takes between 1 and 5 min (48–50) and, in *S. elongatus* UTEX 3055, around 1 min (34), which is similar to the 1 to 2 min observed for OS-A and OS-B′. The motility bias reported in these organisms varies within and between studies but averages about 0.4 (34, 48–50), which is similar to the bias observed in OS-A and twice as high as that of OS-B′.

We observed that light quality, intensity, cell density, and agarose percentage affected collective behavior in terms of the length and appearance of phototactic projections (Fig. 4 and 5; Fig. S6). For example, higher cell densities and light intensities that induced greater bias led to the development of a more uniform front of cells rather than finger-like projections. This is consistent with results described for *Synechocystis* (29, 49) as well as those predicted by reaction-diffusion model simulations (31). As described for *Synechocystis*, cell density affects incident light levels, the

TABLE 2 Comparison of phototactic phenotypes and phototaxis photoreceptors in selected unicellular cyanobacteria[a]

Isolate/species	Environment	Photokinesis	Positive phototaxis (bias value)	Negative phototaxis	Optimal intensity for phototaxis	Phototaxis photoreceptors
Synechococcus OS-A	Hot spring (36, 39)	Yes	Yes (0.3)	Yes (transient)	40-80 μmol·m^{-2}·s^{-1}	UirS
Synechococcus OS-B′	Hot spring (36, 39)	No	Yes (0.2)	Yes (very transient)	10-20 μmol·m^{-2}·s^{-1}	UirS
Synechococcus C1	Hot spring (16)	Yes (16)	Yes (nd) (16)	Yes (16)	nd (16)	nd (16)
Synechococcus C9	Hot spring (16)	Yes (16)	Yes (nd) (16)	Yes (16)	nd (16)	nd (16)
T. elongatus BP1	Hot spring (78, 79)	No (47)	Yes (nd) (47)	No (47)	25–100 μmol·m^{-2}·s^{-1} (47)	PixJ, PixD (80, 81)
T. vulcanus NIES-2134	Hot spring (35)	ND (35)	Yes (nd) (35)	Yes (35)	70 μmol·m^{-2}·s^{-1} (35)	PixD (35)
S. elongatus UTEX 3055	Stream (34)	ND (34)	Yes (0.35) (34)	Yes (34)	20 μmol·m^{-2}·s^{-1} (34)	PixJ (34)
Synechocystis PCC 6803	Freshwater lake (82)	Yes (49, 52)	Yes (0.5) (49, 50, 52)	Yes (24, 49, 83)	1-10 μmol·m^{-2}·s^{-1} (52)	PixD, PixJ, UirS (24, 25, 83)

[a]ND, not determined.

concentration of released exopolysaccharides in the local environment, and physical interactions between cells, suggesting that the action of individual cells leads to the collective formation of phototactic projections (32, 33, 51).

In *Synechocystis*, high-intensity white light and UVA consistently elicited negative phototaxis (24, 52), and mutants with mutations in the photoreceptors PixJ and UirS as well as the pilus retraction ATPase PilT2 exhibited inverted phototactic responses, indicating their role in phototaxis decision-making (22, 24, 46, 52). Negative phototaxis in OS-A appeared to be a transient phenomenon that generally appeared earlier than positive phototaxis. This is similar to *Synechococcus* C1, which also formed negative projections initiating prior to but continuing in parallel with the positive projections (16). Our results (Fig. 3, 5, and 6) suggest that this negative phototactic response may serve as an initial strategy to reduce high light exposure and so avoid the damaging effects of excessive ROS production, but further experiments will be needed to test this.

Green (520 nm) and red (630 nm) light had the strongest effect on collective phototaxis in both OS-A and OS-B′. UVA (360 nm) and blue (450 nm) radiation induced minimal collective phototaxis in OS-B′ and none in OS-A. These results closely reflect what has been shown in *Synechocystis* and *T. elongatus* (29, 34, 47). OS-A and OS-B′ were most phototactic toward red light of low intensities but showed greater collective motility under green light at higher intensities (Fig. 4). This response is similar to that observed in *Synechocystis* (49, 52) but not in the *S. elongatus* isolate UTEX 3055, which performs only positive phototaxis under low blue light and negative phototaxis under high blue light (34). This is what we observed in the short-term single-cell phototactic responses of OS-A and OS-B′ (Fig. S6), where the transition from positive to negative phototaxis occurred at approximately 35 μmol·m^{-2}·s^{-1} for OS-B′ and 65 μmol·m^{-2}·s^{-1} for OS-A. *T. vulcanus*, on the other hand, switches direction from positive phototaxis under green illumination to negative phototaxis as the proportion of blue light is increased (35). The fact that OS-A and OS-B′ have a negative phototaxis phenotype when initially exposed to high-intensity blue light but do not form negative finger-like projections is perhaps surprising but was also observed in *Synechocystis* (25, 29). Because single-cell speed is lower under high-intensity blue than red or green light while phototactic bias is still high, it is likely that motility rather than phototactic bias is inhibited over long time periods and hence prevents the formation of negative phototactic projections.

Genes required for phototaxis in OS-A and OS-B′ compared to other cyanobacteria. To connect the phototactic behaviors of OS-A and OS-B′ to their gene repertoire, we analyzed their phototaxis-related homologs based on genes characterized in *Synechocystis*. The lack of bilin-binding cysteines in the GAF domains of PixJ in OS-A and OS-B′, as well as the insertion of an ISSoc1 transposase in OS-A (OS-A and OS-B′ are known to have several active transposons that disrupt gene function [36, 53]), suggests that PixJ is unlikely to be functional. *T. vulcanus* has also been found to lack PixJ entirely and yet shows both positive and negative phototaxis under green and teal light, respectively (35). A second blue-light photoreceptor, PixD, promotes positive phototaxis in *Synechocystis*, but in *T. vulcanus*, *pixD* mutants do not exhibit a loss of positive phototaxis (25, 35). OS-A and OS-B′ lack a homolog of PixD. Therefore, of the three phototaxis-related directional photoreceptors characterized in *Synechocystis*, the putative UirS homolog is the most likely to be functional in OS-A and OS-B′ (24).

In OS-B′, the first GAF domain of UirS contains both conserved bilin-binding cysteines, but in OS-A, it contains only the "canonical" Cys; the second Cys is substituted by Tyr. Studies of the cyanobacterium *Acaryochloris marina* have revealed that this second cysteine is dispensable for isomerization of phycocyanobilin to phycoviolobilin (54), and the Tyr residue is conserved in red/green cyanobacteriochromes of *Anabaena* and *Synechocystis* (55) as well as in phytochromes more broadly (56). This Cys-to-Tyr substitution in OS-A may be responsible for its reduced collective response relative to OS-B′ under blue and UVA radiation by shifting the absorption to longer wavelengths (57, 58). It may also explain their different light intensity optima for positive phototaxis (higher for OS-A than OS-B′). The duplications of the PAS, PAC, and GAF domains in the UirS homologs in both OS-A and OS-B′ suggest an expanded role for this protein.

In UTEX 3055, which has no UirS homolog, the PixJ homolog has five GAF domains that control both positive and negative phototaxis (34). Multiple PAS/PAC and GAF domains are common in cyanobacteria and may amplify the sensory signal (59).

Based on our analysis, the pilus apparatus and phototaxis signal transduction components, such as the ATPases PilB1 and PilT1, and the CheY-like response regulators PilI/PixG/PixH are highly conserved (Table S2) (23). However, the repertoire of photoreceptors appears to be more diverse (60). This may reflect the different light environments that cyanobacteria inhabit, where light intensity and quality are a function of the weather conditions, the time of day and year, the depth in the microbial mat, and the density of other co-occurring, light-absorbing community members.

Linking phototaxis in OS-A and OS-B′ with *in situ* studies of light-dependent motility in Yellowstone microbial mats. Light intensity and quality can change rapidly, such as on a cloudy day (61), and our results indicate that *Synechococcus* cells can respond rapidly (Fig. 2). In filamentous cyanobacteria, uncouplers of oxidative phosphorylation and ATP addition alter cell motility (62), and so it seems plausible that changes in light intensity would rapidly affect photosynthetic electron transport, ATP levels, and hence impact motility. The transient peak in OS-A speed on illumination and transient dip in OS-B′ speed on transition to darkness might be associated with the delay in activation and deactivation of the Calvin cycle (an ATP sink) that is known to occur with similar timescales during light transitions (63, 64). However, uncovering the integration of photosynthesis and light-dependent motility and determining why OS-A and OS-B′ show different motility dynamics during light transitions will require further experimentation.

The often-high density of cyanobacteria at the mat surface can attenuate blue light by 99% within the top millimeter (4). If the rate of movement that we observed of 350 to 700 μm·h^{-1} with a phototactic bias of 0.2 to 0.4 is of the same order of magnitude as in the mat, then it is plausible that phototaxis can help to optimize light exposure over the diel cycle. Ramsing et al. (12) found that the vertical distribution of OS-A relative to OS-B′ changed over the day, with a greater abundance of OS-A near the surface at midday than predawn (4:00 a.m.). Based on our results (Fig. 3 and 5), we hypothesize that in the morning, when light intensity is low, OS-B′ would show positive phototaxis toward the surface. As light intensity increases, however, OS-B′ may reverse its direction. As more green light penetrates the mat, it may promote the movement of OS-A upward toward the light, leaving it nearer the surface at midday. As light intensity decreases over the afternoon, OS-B′ may once again show greater bias toward the surface and dominate the upper layers by late afternoon and overnight. Ramsing et al. (12) also observed that cells at a depth of 600 to 800 μm (mostly OS-A) are predominantly vertically oriented. Our results indicate that OS-A and OS-B′ move mostly along their long axis, and so the observed vertical orientation is consistent with both vertical migration of cells through the mat and rotation of cells in place to change the cell surface area exposed to light. It will also be interesting to check if OS-A and OS-B′ move in response to other gradients, such as temperature (65), pH (66), O_2 (67, 68) or various organic compounds (69).

Phototaxis may allow *Synechococcus* sp. to laterally colonize new areas of the mat as new niches are created by erosion, biofilm growth, and seasonal changes in temperature and insulation or when damage to the mat occurs. Indeed, *Synechococcus* rapidly recolonized Mushroom Spring after hailstorm damage (70), and after artificial removal of the top 3 mm of the Octopus Spring mat, the colonizing *Synechococcus* community differed substantially from the removed community, with the fastest colonization by OS-A, -A′, and -A′′′ ecotypes (39). As we found that OS-A had a higher light intensity optimum for positive phototaxis (Fig. 3), it is plausible that these strains were the first to colonize the disrupted area because they also have higher light intensity optima for phototaxis.

Conclusions. *Synechococcus* isolates representative of the dominant cyanobacterial species in Octopus and Mushroom thermal springs are phototactic but exhibit key differences in their light-induced motility. OS-A shows positive photokinesis on

illumination and a greater phototactic bias than OS-B′. OS-A is less responsive to low-intensity light and more positively phototactic at higher intensities than OS-B′, and yet it performs negative collective phototaxis even at relatively low intensities, whereas OS-B′ very rarely displays this phenotype. These differences allow OS-A and OS-B′ to segregate according to light intensity and suggest that phototaxis may partly explain why the abundance of *Synechococcus* ecotypes varies so substantially with depth. Similar to *Synechocystis*, these isolates are most sensitive to red and green light and show minimal collective phototaxis under blue light or UVA, but at the single-cell level over short timescales, blue light has the greatest effect, inducing a switch from positive to negative phototaxis as the intensity is increased. The molecular determinants of these differences are unclear, but a putative homolog of the UirS photoreceptor, found in both isolates but with important differences in their bilin-binding residues, may play a critical role. These differences at the genetic and phenotypic levels in two of the major cyanobacteria in these biofilms hint at a greater diversity in the growth and survival strategies of thermophilic cyanobacteria in this environment.

MATERIALS AND METHODS

Strains and culture conditions. *Synechococcus* sp. JA-3-3Ab (OS-A) and *Synechococcus* sp. JA-2-3B′a (2-13) (OS-B′) were originally isolated by filter cultivation from Octopus Spring mat samples between 58 and 65°C and 51 to 61°C, respectively (36, 37). Strains were stored at −70°C in 20% (vol/vol) glycerol stocks prior to culturing. Culturing was generally performed in 50 mL of DH10 medium (medium D [71] plus 10 mM HEPES) adjusted to pH 8.2 with 250 mg·L^{-1} tryptone in 150-mL conical flasks at 50°C under 12:12 light-dark cycles with a light intensity of 50 μmol·m^{-2}·s^{-1} (measured with a LI-COR [model Li-189] radiometer) in an Algaetron ag130 incubator (Photon Systems Instruments) or in a homemade incubator under the same light intensity, light period, and temperature conditions. To determine if cultures were axenic, we observed them under the microscope after plating them on DH10 agarose plates with added tryptone (100 mg/L) and yeast extract (100 mg/L) and checking for the absence of any non-*Synechococcus* colonies. There have been recent proposals to reclassify and rename *Synechococcus* sp. strain JA-3-3Ab (NCBI taxid 321327) and *Synechococcus* sp. strain JA-2-3B′a(2-13) (NCBI taxid 321332) in the genera *Leptococcus* (72) and *Thermostichus* (73, 74). However, here we use the original nomenclature to stay consistent with our previous publications.

Collective phototaxis measurements. The standard parameters for phototaxis experiments started with cultures in late log phase (OD_{730} of OS-A, ~0.4; OD_{730} of OS-B′, ~0.6). Five microliters of the cultures, adjusted to an OD_{730} of 8.0 by using a spectrophotometer (Tecan M1000 Pro) and concentrating the culture by centrifugation, supernatant removal, and resuspension in a calculated volume of DH10, was plated on DH10 medium solidified with 0.4% (wt/vol) agarose in bacteriological petri dishes with tightly fitting lids (Falcon 25369-022) and allowed to dry for approximately 10 min in a laminar flow cabinet. Plates were then incubated (agar side up) at 50°C with unidirectional daylight white LED illumination (spectrum in Fig. S1A) at 60 μmol·m^{2}·s^{-1}. Measurements of the extension of phototactic "fingers" were recorded using a ruler, every 24 h for 10 days from the original edge of the droplet closest to the light to the tip of the longest phototactic finger. Results were analyzed using R version 4.0.5.

Microscope-based single-cell phototaxis measurements. For single-cell motility measurements by TLVM, the temperature was maintained at 50°C using a custom environmental chamber (HaisonTech). Illumination was provided by rows of warm and daylight white LEDs (spectra in Fig. S1) positioned 10 cm from and at an angle of 5 to 10° above the agarose surface. The measured light intensity at the cells' position was 70 μmol·m^{2}·s^{-1}. Cells were prepared as described above for collective phototaxis measurements and recorded from within the phototactic projections after 2 to 5 days incubation under directional white light. All petri dishes remained closed and inverted during recording with a minimum of 20 min incubation at 50°C and 5 min of darkness prior to the 4- to 10-min recordings at ×200 magnification and 10 frames per min. All movies were made using a Nikon Eclipse TE300 inverted microscope attached to a Coolsnap Pro monochrome camera (Media Cybernetics, Silver Spring, MD, USA), and images were collected by MetaMorph software (v4.6r5 and 6.2r6; Molecular Devices). Example videos can be found at https://www.youtube.com/channel/UCX0gm-79tZplREzHteapEWA. Image stacks were preprocessed using Image J v1.53f51 (75) by subtracting the background with a rolling ball radius of 4. Cells were tracked using the ImageJ plugin Trackmate (76) with a thresholding filter applied and filtering to blobs of >25 pixels. The Kalman tracker was selected with the initial search radius set to 15, the search radius to 15, and the maximum frame gap to 3. The "spots" file was exported to csv and imported into R version 4.0.5 for preprocessing and analysis. Tracks consisting of fewer than 5 frames (25 s) were discarded. For Fig. 1 and for Fig. S3 and S4, speed and motility bias were calculated per cell over the full length of their track, whereas for Fig. 2 and Fig. S6, speed and motility bias were calculated for each 6-s time interval. Speed was calculated as distance (in μm)/time (in s). Motility bias was calculated as parallel displacement (in μm)/distance (in μm). Rayleigh and Kolmogorov-Smirnov tests were performed using the "rayleigh.test" and "ks.test" functions from the "Directional" and "stats" packages, respectively.

Isolate quantification by qPCR. Following the phototaxis experiment whose results are shown in Fig. 5A, cells were picked using 200-μL pipette tips from a 1- to 2-mm-wide cross-section of the phototactic finger-like projections (Fig. 5A) and transferred to 5 μL of DH10 medium in a 96-well PCR plate.

Twenty microliters of 20 mM NaOH was added to each well, and the cells were frozen for at least 10 min in a −70°C freezer. The plate was then heated at 98°C in a thermocycler for 5 min, followed immediately by the addition of 100 μL of distilled H_2O, chilling on ice, and preparation of the qPCR. Five microliters of the cell lysate was added to a qPCR plate, followed by 6 μL of a master mix composed of 5 μL 2× SensiFAST SYBR No-ROX kit reaction mix (Meridian Bioscience; BIO-98050) plus 0.5 μL of each 10 mM primer stock (Table 1). PCR amplification was performed over 45 cycles of 95°C for 10 s and 60°C for 30 s, followed by melting curve analysis by ramping the temperature from 65°C to 97°C at 0.11°C per second. A 2-fold dilution series of OS-A and OS-B′ over a 128-fold range was also tested to define the relationship between cell density and PCR threshold cycle value, and target specificity was confirmed by observing no amplification of the nontarget cell extract and a single peak in the melt profile. The nonparametric Kruskal-Wallis [kruskal.test() in the stats package] and *post hoc* Dunn's [dunn_test() in the rstatix package] tests (with Benjamini-Hochberg correction) were performed to determine the statistical differences between all comparisons of group (positions 1 to 5 in Fig. 5) medians, and the results are displayed in Fig. 5 using a compact letter display.

Homolog identification. Gene homologs were identified in OS-A (*Synechococcus* sp. strain JA-3-3Ab; NCBI taxid 321327) and OS-B′ [*Synechococcus* sp. strain JA-2-3B′a(2-13); NCBI taxid 321332] genomes using *Synechocystis* sp. strain PCC 6803 (GenBank accession no. GCA_000009725.1) proteins as queries (listed in Table S2). A reciprocal BLASTp approach was conducted to identify putative orthologs in both isolates. Each protein sequence of interest in *Synechocystis* was used as a query for a BLAST search using Geneious Prime 2020.1.1 with default settings against each OS-A and OS-B′ genome, and the resulting top three hits were then BLAST searched against *Synechocystis* to confirm their homology using the GenomeNet BLAST search tool (https://www.genome.jp/tools/blast/). If the resulting best hit in *Synechocystis* obtained in the second BLAST search matched the sequence used as a query in the first BLAST search, the corresponding sequence in OS-A or OS-B′ was considered a putative ortholog candidate. Additionally, the presence of conserved protein domains was considered when assigning a putative ortholog. Therefore, the resulting candidates from the reciprocal BLAST search were analyzed for conserved domains using the online Simple Modular Architecture Research Tool (SMART) (77), and putative orthologs in OS-A and OS-B′ were considered only when these proteins showed at least one copy for each of the conserved domains in the corresponding *Synechocystis* protein query.

SUPPLEMENTAL MATERIAL

Supplemental material is available online only.

SUPPLEMENTAL FILE 1, PDF file, 1 MB.

SUPPLEMENTAL FILE 2, XLSX file, 0.01 MB.

ACKNOWLEDGMENTS

F.B., A.N.S., and C.R. were supported by a BBSRC-NSF/BIO collaborative research grant (award number 1921429) and the Carnegie Institution for Science. D.B. and A.G. acknowledge support from NSF/BIO award number 1921429 and from the Carnegie Institution for Science. V.C. is supported by a grant from the National Aeronautics and Space Administration (80NSSC19K0462).

We thank the Yellowstone National Park Service and David Ward for sampling permit #YELL-5494 awarded to David Ward and Devaki Bhaya, which allowed the collection of mat samples from which OS-A and OS-B' were isolated.

F.B. and D.B. conceived and designed the research. F.B., C.R., and V.C. carried out experiments. F.B. and D.B. wrote the initial manuscript. F.B., D.B., A.G., C.R., V.C., and A.N.S. analyzed the results and edited the manuscript.

REFERENCES

1. Ward DM, Ferris MJ, Nold SC, Bateson MM. 1998. A natural view of microbial biodiversity within hot spring cyanobacterial mat communities. Microbiol Mol Biol Rev 62:1353–1370. https://doi.org/10.1128/MMBR.62.4.1353-1370.1998.
2. Thiel V, Hügler M, Ward DM, Bryant DA. 2017. The dark side of the Mushroom Spring microbial mat: life in the shadow of chlorophototrophs. II. Metabolic functions of abundant community members predicted from metagenomic analyses. Front Microbiol 8:943. https://doi.org/10.3389/fmicb.2017.00943.
3. Revsbech NP, Ward DM. 1984. Microelectrode studies of interstitial water chemistry and photosynthetic activity in a hot spring microbial mat. Appl Environ Microbiol 48:270–275. https://doi.org/10.1128/aem.48.2.270-275.1984.
4. Ferris MJ, Kühl M, Wieland A, Ward DM. 2003. Cyanobacterial ecotypes in different optical microenvironments of a 68°C hot spring mat community revealed by 16S-23S rRNA internal transcribed spacer region variation. Appl Environ Microbiol 69:2893–2898. https://doi.org/10.1128/AEM.69.5.2893-2898.2003.
5. Becraft ED, Wood JM, Rusch DB, Kühl M, Jensen SI, Bryant DA, Roberts DW, Cohan FM, Ward DM. 2015. The molecular dimension of microbial species: 1. Ecological distinctions among, and homogeneity within, putative ecotypes of Synechococcus inhabiting the cyanobacterial mat of Mushroom Spring, Yellowstone National Park. Front Microbiol 6:590. https://doi.org/10.3389/fmicb.2015.00590.
6. Klatt CG, Wood JM, Rusch DB, Bateson MM, Hamamura N, Heidelberg JF, Grossman AR, Bhaya D, Cohan FM, Kühl M, Bryant DA, Ward DM. 2011. Community ecology of hot spring cyanobacterial mats: predominant populations and their functional potential. ISME J 5:1262–1278. https://doi.org/10.1038/ismej.2011.73.
7. Ferris MJ, Ward DM. 1997. Seasonal distributions of dominant 16S rRNA-defined populations in a hot spring microbial mat examined by

denaturing gradient gel electrophoresis. Appl Environ Microbiol 63:1375–1381. https://doi.org/10.1128/aem.63.4.1375-1381.1997.
8. Nübel U, Bateson MM, Vandieken V, Wieland A, Kühl M, Ward DM. 2002. Microscopic examination of distribution and phenotypic properties of phylogenetically diverse Chloroflexaceae-related bacteria in hot spring microbial mats. Appl Environ Microbiol 68:4593–4603. https://doi.org/10.1128/AEM.68.9.4593-4603.2002.
9. Kim Y-M, Nowack S, Olsen MT, Becraft ED, Wood JM, Thiel V, Klapper I, Kühl M, Fredrickson JK, Bryant DA, Ward DM, Metz TO. 2015. Diel metabolomics analysis of a hot spring chlorophototrophic microbial mat leads to new hypotheses of community member metabolisms. Front Microbiol 6:209. https://doi.org/10.3389/fmicb.2015.00209.
10. Steunou A-S, Bhaya D, Bateson MM, Melendrez MC, Ward DM, Brecht E, Peters JW, Kühl M, Grossman AR. 2006. In situ analysis of nitrogen fixation and metabolic switching in unicellular thermophilic cyanobacteria inhabiting hot spring microbial mats. Proc Natl Acad Sci U S A 103:2398–2403. https://doi.org/10.1073/pnas.0507513103.
11. Jensen SI, Steunou A-S, Bhaya D, Kühl M, Grossman AR. 2011. In situ dynamics of O2, pH and cyanobacterial transcripts associated with CCM, photosynthesis and detoxification of ROS. ISME J 5:317–328. https://doi.org/10.1038/ismej.2010.131.
12. Ramsing NB, Ferris MJ, Ward DM. 2000. Highly ordered vertical structure of Synechococcus populations within the one-millimeter-thick photic zone of a hot spring cyanobacterial mat. Appl Environ Microbiol 66:1038–1049. https://doi.org/10.1128/AEM.66.3.1038-1049.2000.
13. Nowack S, Olsen MT, Schaible GA, Becraft ED, Shen G, Klapper I, Bryant DA, Ward DM. 2015. The molecular dimension of microbial species: 2. Synechococcus strains representative of putative ecotypes inhabiting different depths in the Mushroom Spring microbial mat exhibit different adaptive and acclimative responses to light. Front Microbiol 6:626. https://doi.org/10.3389/fmicb.2015.00626.
14. Brock TD. 1978. Thermophilic microorganisms and life at high temperatures. Springer, New York, NY.
15. Carr NG, Whitton BA. 1973. The biology of blue-green algae. University of California Press, Berkeley, CA.
16. Ramsing NB, Ferris MJ, Ward DM. 1997. Light-induced motility of thermophilic Synechococcus isolates from Octopus Spring, Yellowstone National Park. Appl Environ Microbiol 63:2347–2354. https://doi.org/10.1128/aem.63.6.2347-2354.1997.
17. Tank M, Thiel V, Ward DM, Bryant DA. 2017. A panoply of phototrophs: an overview of the thermophilic chlorophototrophs of the microbial mats of alkaline siliceous hot springs in Yellowstone National Park, WY, USA, p 87–137. *In* Hallenbeck PC (ed), Modern topics in the phototrophic prokaryotes: environmental and applied aspects. Springer International Publishing, Cham, Switzerland.
18. Ferris MJ, Ruff-Roberts AL, Kopczynski ED, Bateson MM, Ward DM. 1996. Enrichment culture and microscopy conceal diverse thermophilic Synechococcus populations in a single hot spring microbial mat habitat. Appl Environ Microbiol 62:1045–1050. https://doi.org/10.1128/aem.62.3.1045-1050.1996.
19. Bhaya D, Takahashi A, Grossman AR. 2001. Light regulation of type IV pilus-dependent motility by chemosensor-like elements in Synechocystis PCC6803. Proc Natl Acad Sci U S A 98:7540–7545. https://doi.org/10.1073/pnas.131201098.
20. Schuergers N, Mullineaux CW, Wilde A. 2017. Cyanobacteria in motion. Curr Opin Plant Biol 37:109–115. https://doi.org/10.1016/j.pbi.2017.03.018.
21. Schuergers N, Lenn T, Kampmann R, Meissner MV, Esteves T, Temerinac-Ott M, Korvink JG, Lowe AR, Mullineaux CW, Wilde A. 2016. Cyanobacteria use micro-optics to sense light direction. Elife 5:e12620. https://doi.org/10.7554/eLife.12620.
22. Bhaya D, Bianco NR, Bryant D, Grossman A. 2000. Type IV pilus biogenesis and motility in the cyanobacterium Synechocystis sp. PCC6803. Mol Microbiol 37:941–951. https://doi.org/10.1046/j.1365-2958.2000.02068.x.
23. Wilde A, Mullineaux CW. 2017. Light-controlled motility in prokaryotes and the problem of directional light perception. FEMS Microbiol Rev 41:900–922. https://doi.org/10.1093/femsre/fux045.
24. Song J-Y, Cho HS, Cho J-I, Jeon J-S, Lagarias JC, Park Y-I. 2011. Near-UV cyanobacteriochrome signaling system elicits negative phototaxis in the cyanobacterium Synechocystis sp. PCC 6803. Proc Natl Acad Sci U S A 108:10780–10785. https://doi.org/10.1073/pnas.1104242108.
25. Sugimoto Y, Nakamura H, Ren S, Hori K, Masuda S. 2017. Genetics of the blue light-dependent signal cascade that controls phototaxis in the cyanobacterium Synechocystis sp. PCC6803. Plant Cell Physiol 58:458–465. https://doi.org/10.1093/pcp/pcw218.
26. Terauchi K, Ohmori M. 2004. Blue light stimulates cyanobacterial motility via a cAMP signal transduction system. Mol Microbiol 52:303–309. https://doi.org/10.1111/j.1365-2958.2003.03980.x.
27. Savakis P, De Causmaecker S, Angerer V, Ruppert U, Anders K, Essen L-O, Wilde A. 2012. Light-induced alteration of c-di-GMP level controls motility of Synechocystis sp. PCC 6803. Mol Microbiol 85:239–251. https://doi.org/10.1111/j.1365-2958.2012.08106.x.
28. Masuda S, Ono T-A. 2004. Biochemical characterization of the major adenylyl cyclase, Cya1, in the cyanobacterium Synechocystis sp. PCC 6803. FEBS Lett 577:255–258. https://doi.org/10.1016/j.febslet.2004.09.086.
29. Bhaya D, Nakasugi K, Fazeli F, Burriesci MS. 2006. Phototaxis and impaired motility in adenylyl cyclase and cyclase receptor protein mutants of Synechocystis sp. strain PCC 6803. J Bacteriol 188:7306–7310. https://doi.org/10.1128/JB.00573-06.
30. Wallner T, Pedroza L, Voigt K, Kaever V, Wilde A. 2020. The cyanobacterial phytochrome 2 regulates the expression of motility-related genes through the second messenger cyclic di-GMP. Photochem Photobiol Sci 19:631–643. https://doi.org/10.1039/c9pp00489k.
31. Ursell T, Chau RMW, Wisen S, Bhaya D, Huang KC. 2013. Motility enhancement through surface modification is sufficient for cyanobacterial community organization during phototaxis. PLoS Comput Biol 9:e1003205. https://doi.org/10.1371/journal.pcbi.1003205.
32. Burriesci M, Bhaya D. 2008. Tracking phototactic responses and modeling motility of Synechocystis sp. strain PCC6803. J Photochem Photobiol B 91:77–86. https://doi.org/10.1016/j.jphotobiol.2008.01.012.
33. Varuni P, Menon SN, Menon GI. 2017. Phototaxis as a collective phenomenon in cyanobacterial colonies. Sci Rep 7:17799. https://doi.org/10.1038/s41598-017-18160-w.
34. Yang Y, Lam V, Adomako M, Simkovsky R, Jakob A, Rockwell NC, Cohen SE, Taton A, Wang J, Lagarias JC, Wilde A, Nobles DR, Brand JJ, Golden SS. 2018. Phototaxis in a wild isolate of the cyanobacterium Synechococcus elongatus. Proc Natl Acad Sci U S A 115:E12378–E12387. https://doi.org/10.1073/pnas.1812871115.
35. Nakane D, Enomoto G, Wilde A, Nishizaka T. 2021. Thermosynechococcus switches the direction of phototaxis by a c-di-GMP dependent process with high spatial resolution. bioRxiv. https://doi.org/10.1101/2021.08.26.457869.
36. Bhaya D, Grossman AR, Steunou A-S, Khuri N, Cohan FM, Hamamura N, Melendrez MC, Bateson MM, Ward DM, Heidelberg JF. 2007. Population level functional diversity in a microbial community revealed by comparative genomic and metagenomic analyses. ISME J 1:703–713. https://doi.org/10.1038/ismej.2007.46.
37. Allewalt JP, Bateson MM, Revsbech NP, Slack K, Ward DM. 2006. Effect of temperature and light on growth of and photosynthesis by Synechococcus isolates typical of those predominating in the Octopus Spring microbial mat community of Yellowstone National Park. Appl Environ Microbiol 72:544–550. https://doi.org/10.1128/AEM.72.1.544-550.2006.
38. Kilian O, Steunou A-S, Fazeli F, Bailey S, Bhaya D, Grossman AR. 2007. Responses of a thermophilic Synechococcus isolate from the microbial mat of Octopus Spring to light. Appl Environ Microbiol 73:4268–4278. https://doi.org/10.1128/AEM.00201-07.
39. Ferris MJ, Nold SC, Revsbech NP, Ward DM. 1997. Population structure and physiological changes within a hot spring microbial mat community following disturbance. Appl Environ Microbiol 63:1367–1374. https://doi.org/10.1128/aem.63.4.1367-1374.1997.
40. Menon SN, Varuni P, Bunbury F, Bhaya D, Menon GI. 2021. Phototaxis in cyanobacteria: from mutants to models of collective behavior. mBio 12:e02398-21. https://doi.org/10.1128/mBio.02398-21.
41. Yuan H, Bauer CE. 2008. PixE promotes dark oligomerization of the BLUF photoreceptor PixD. Proc Natl Acad Sci U S A 105:11715–11719. https://doi.org/10.1073/pnas.0802149105.
42. Bhaya D. 2004. Light matters: phototaxis and signal transduction in unicellular cyanobacteria. Mol Microbiol 53:745–754. https://doi.org/10.1111/j.1365-2958.2004.04160.x.
43. El Mouali Y, Kim H, Ahmad I, Brauner A, Liu Y, Skurnik M, Galperin MY, Römling U. 2017. Stand-alone EAL domain proteins form a distinct subclass of EAL proteins involved in regulation of cell motility and biofilm formation in Enterobacteria. J Bacteriol 199:e00179-17. https://doi.org/10.1128/JB.00179-17.
44. Ulijasz AT, Cornilescu G, von Stetten D, Cornilescu C, Escobar FV, Zhang J, Stankey RJ, Rivera M, Hildebrandt P, Vierstra RD. 2009. Cyanochromes are blue/green light photoreversible photoreceptors defined by a stable double cysteine linkage to a phycoviolobilin-type chromophore. J Biol Chem 284:29757–29772. https://doi.org/10.1074/jbc.M109.038513.

45. Rockwell NC, Njuguna SL, Roberts L, Castillo E, Parson VL, Dwojak S, Lagarias JC, Spiller SC. 2008. A second conserved GAF domain cysteine is required for the blue/green photoreversibility of cyanobacteriochrome Tlr0924 from Thermosynechococcus elongatus. Biochemistry 47:7304–7316. https://doi.org/10.1021/bi800088t.
46. Narikawa R, Suzuki F, Yoshihara S, Higashi S-I, Watanabe M, Ikeuchi M. 2011. Novel photosensory two-component system (PixA-NixB-NixC) involved in the regulation of positive and negative phototaxis of cyanobacterium Synechocystis sp. PCC 6803. Plant Cell Physiol 52:2214–2224. https://doi.org/10.1093/pcp/pcr155.
47. Kondou Y, Nakazawa M, Higashi S-I, Watanabe M, Manabe K. 2007. Equal -quantum action spectra indicate fluence-rate-selective action of multiple photoreceptors for photomovement of the thermophilic cyanobacterium Synechococcus elongatus. Photochem Photobiol 73:90–95. https://doi.org/10.1562/0031-8655(2001)0730090EQASIF2.0.CO2.
48. Chau RMW, Bhaya D, Huang KC. 2017. Emergent phototactic responses of cyanobacteria under complex light regimes. mBio 8:e02330-16. https://doi.org/10.1128/mBio.02330-16.
49. Choi J-S, Chung Y-H, Moon Y-J, Kim C, Watanabe M, Song P-S, Joe C-O, Bogorad L, Park YM. 1999. Photomovement of the gliding cyanobacterium Synechocystis sp. PCC 6803. Photochem Photobiol 70:95–102. https://doi.org/10.1111/j.1751-1097.1999.tb01954.x.
50. Chau RMW, Ursell T, Wang S, Huang KC, Bhaya D. 2015. Maintenance of motility bias during cyanobacterial phototaxis. Biophys J 108:1623–1632. https://doi.org/10.1016/j.bpj.2015.01.042.
51. Wilde A, Mullineaux CW. 2015. Motility in cyanobacteria: polysaccharide tracks and Type IV pilus motors. Mol Microbiol 98:998–1001. https://doi.org/10.1111/mmi.13242.
52. Ng W-O, Grossman AR, Bhaya D. 2003. Multiple light inputs control phototaxis in Synechocystis sp. strain PCC6803. J Bacteriol 185:1599–1607. https://doi.org/10.1128/JB.185.5.1599-1607.2003.
53. Nelson WC, Bhaya D, Heidelberg JF. 2012. Novel miniature transposable elements in thermophilic Synechococcus strains and their impact on an environmental population. J Bacteriol 194:3636–3642. https://doi.org/10.1128/JB.00333-12.
54. Fushimi K, Narikawa R. 2021. Unusual ring D fixation by three crucial residues promotes phycoviolobilin formation in the DXCF-type cyanobacteriochrome without the second Cys. Biochem J 478:1043–1059. https://doi.org/10.1042/BCJ20210013.
55. Sato T, Kikukawa T, Miyoshi R, Kajimoto K, Yonekawa C, Fujisawa T, Unno M, Eki T, Hirose Y. 2019. Protochromic absorption changes in the two-cysteine photocycle of a blue/orange cyanobacteriochrome. J Biol Chem 294:18909–18922. https://doi.org/10.1074/jbc.RA119.010384.
56. Fischer AJ, Rockwell NC, Jang AY, Ernst LA, Waggoner AS, Duan Y, Lei H, Lagarias JC. 2005. Multiple roles of a conserved GAF domain tyrosine residue in cyanobacterial and plant phytochromes. Biochemistry 44:15203–15215. https://doi.org/10.1021/bi051633z.
57. Hontani Y, Shcherbakova DM, Baloban M, Zhu J, Verkhusha VV, Kennis JTM. 2016. Bright blue-shifted fluorescent proteins with Cys in the GAF domain engineered from bacterial phytochromes: fluorescence mechanisms and excited-state dynamics. Sci Rep 6:37362. https://doi.org/10.1038/srep37362.
58. Song J-Y, Lee HY, Yang HW, Song J-J, Lagarias JC, Park Y-I. 2020. Spectral and photochemical diversity of tandem cysteine cyanobacterial phytochromes. J Biol Chem 295:6754–6766. https://doi.org/10.1074/jbc.RA120.012950.
59. Taylor BL, Zhulin IB. 1999. PAS domains: internal sensors of oxygen, redox potential, and light. Microbiol Mol Biol Rev 63:479–506. https://doi.org/10.1128/MMBR.63.2.479-506.1999.
60. Wiltbank LB, Kehoe DM. 2019. Diverse light responses of cyanobacteria mediated by phytochrome superfamily photoreceptors. Nat Rev Microbiol 17:37–50. https://doi.org/10.1038/s41579-018-0110-4.
61. Reinhardt K, Smith WK, Carter GA. 2010. Clouds and cloud immersion alter photosynthetic light quality in a temperate mountain cloud forest. Botany 88:462–470. https://doi.org/10.1139/B10-008.
62. Häder DP. 1987. Photosensory behavior in procaryotes. Microbiol Rev 51:1–21. https://doi.org/10.1128/mr.51.1.1-21.1987.
63. Graham PJ, Nguyen B, Burdyny T, Sinton D. 2017. A penalty on photosynthetic growth in fluctuating light. Sci Rep 7:12513. https://doi.org/10.1038/s41598-017-12923-1.
64. Michelet L, Zaffagnini M, Morisse S, Sparla F, Pérez-Pérez ME, Francia F, Danon A, Marchand CH, Fermani S, Trost P, Lemaire SD. 2013. Redox regulation of the Calvin-Benson cycle: something old, something new. Front Plant Sci 4:470. https://doi.org/10.3389/fpls.2013.00470.
65. Paulick A, Jakovljevic V, Zhang S, Erickstad M, Groisman A, Meir Y, Ryu WS, Wingreen NS, Sourjik V. 2017. Mechanism of bidirectional thermotaxis in Escherichia coli. Elife 6:e26607. https://doi.org/10.7554/eLife.26607.
66. Tohidifar P, Plutz MJ, Ordal GW, Rao CV. 2020. The mechanism of bidirectional pH taxis in Bacillus subtilis. J Bacteriol 202:e00491-19. https://doi.org/10.1128/JB.00491-19.
67. Doemel WN, Brock TD. 1977. Structure, growth, and decomposition of laminated algal-bacterial mats in alkaline hot springs. Appl Environ Microbiol 34:433–452. https://doi.org/10.1128/aem.34.4.433-452.1977.
68. Taylor BL, Zhulin IB, Johnson MS. 1999. Aerotaxis and other energy-sensing behavior in bacteria. Annu Rev Microbiol 53:103–128. https://doi.org/10.1146/annurev.micro.53.1.103.
69. Adler J. 1966. Chemotaxis in bacteria. Science 153:708–716. https://doi.org/10.1126/science.153.3737.708.
70. Brock TD, Brock ML. 1969. Recovery of a hot spring community from a catastrophe. J Phycol 5:75–77. https://doi.org/10.1111/j.1529-8817.1969.tb02580.x.
71. Castenholz RW. 1981. Isolation and cultivation of thermophilic cyanobacteria, p 236–246. *In* Starr MP, Stolp H, Trüper HG, Balows A, Schlegel HG (ed), The prokaryotes: a handbook on habitats, isolation, and identification of bacteria. Springer, Berlin, Germany.
72. Walter JM, Coutinho FH, Dutilh BE, Swings J, Thompson FL, Thompson CC. 2017. Ecogenomics and taxonomy of cyanobacteria phylum. Front Microbiol 8:2132. https://doi.org/10.3389/fmicb.2017.02132.
73. Salazar VW, Tschoeke DA, Swings J, Cosenza CA, Mattoso M, Thompson CC, Thompson FL. 2020. A new genomic taxonomy system for the Synechococcus collective. Environ Microbiol 22:4557–4570. https://doi.org/10.1111/1462-2920.15173.
74. Komárek J, Johansen JR, Šmarda J, Strunecký O. 2020. Phylogeny and taxonomy of Synechococcus-like cyanobacteria. Fottea 20:171–191. https://doi.org/10.5507/fot.2020.006.
75. Schindelin J, Arganda-Carreras I, Frise E, Kaynig V, Longair M, Pietzsch T, Preibisch S, Rueden C, Saalfeld S, Schmid B, Tinevez J-Y, White DJ, Hartenstein V, Eliceiri K, Tomancak P, Cardona A. 2012. Fiji: an open-source platform for biological-image analysis. Nat Methods 9:676–682. https://doi.org/10.1038/nmeth.2019.
76. Ershov D, Phan M-S, Pylvänäinen JW, Rigaud SU, Le Blanc L, Charles-Orszag A, Conway JRW, Laine RF, Roy NH, Bonazzi D, Duménil G, Jacquemet G, Tinevez J-Y. 2021. Bringing TrackMate into the era of machine-learning and deep-learning. bioRxiv. https://doi.org/10.1101/2021.09.03.458852.
77. Letunic I, Khedkar S, Bork P. 2021. SMART: recent updates, new developments and status in 2020. Nucleic Acids Res 49:D458–D460. https://doi.org/10.1093/nar/gkaa937.
78. Nakamura Y, Kaneko T, Sato S, Ikeuchi M, Katoh H, Sasamoto S, Watanabe A, Iriguchi M, Kawashima K, Kimura T, Kishida Y, Kiyokawa C, Kohara M, Matsumoto M, Matsuno A, Nakazaki N, Shimpo S, Sugimoto M, Takeuchi C, Yamada M, Tabata S. 2002. Complete genome structure of the thermophilic cyanobacterium Thermosynechococcus elongatus BP-1. DNA Res 9:123–130. https://doi.org/10.1093/dnares/9.4.123.
79. Sacko O, Barnes CL, Greene LH, Lee JW. 2020. Survivability of wild-type and genetically engineered Thermosynechococcus elongatus BP1 with different temperature conditions. Appl Biosaf 25:104–117. https://doi.org/10.1177/1535676019896640.
80. Ishizuka T, Narikawa R, Kohchi T, Katayama M, Ikeuchi M. 2007. Cyanobacteriochrome TePixJ of Thermosynechococcus elongatus harbors phycoviolobilin as a chromophore. Plant Cell Physiol 48:1385–1390. https://doi.org/10.1093/pcp/pcm106.
81. Takahashi R, Okajima K, Suzuki H, Nakamura H, Ikeuchi M, Noguchi T. 2007. FTIR study on the hydrogen bond structure of a key tyrosine residue in the flavin-binding blue light sensor TePixD from Thermosynechococcus elongatus. Biochemistry 46:6459–6467. https://doi.org/10.1021/bi7004653.
82. Yu Y, You L, Liu D, Hollinshead W, Tang YJ, Zhang F. 2013. Development of Synechocystis sp. PCC 6803 as a phototrophic cell factory. Mar Drugs 11:2894–2916. https://doi.org/10.3390/md11082894.
83. Yoshihara S, Katayama M, Geng X, Ikeuchi M. 2004. Cyanobacterial phytochrome-like PixJ1 holoprotein shows novel reversible photoconversion between blue- and green-absorbing forms. Plant Cell Physiol 45:1729–1737. https://doi.org/10.1093/pcp/pch214.